https://doi.org/10.5194/egusphere-2022-1018
Preprint. Discussion started: 18 October 2022

A method to enhance the detecting of geostrophic current and its temporal variations with SWOT swath data

Jiasheng Shi[1], Taoyong Jin[1,2], Mao Zhou[1], Xiangcheng Wan[3], Weiping Jiang[2,4]

[1]MOE Key Laboratory of Geospace Environment and Geodesy, School of Geodesy and Geomatics, Wuhan University, Wuhan, China
[2]Hubei Luojia Laboratory, Wuhan, China
[3]Shanghai Institute of Satellite Engineering, Shanghai, China
[4]GNSS Research Center, Wuhan University, Wuhan, China

Correspondence to: Taoyong Jin (tyjin@sgg.whu.edu.cn)

Abstract. The Surface Water and Ocean Topography (SWOT) mission, which can map the sea surface height with high spatial and temporal sampling rates simultaneously, has significant potential for detecting mesoscale and submesoscale eddy variations. At present, in the determination of geostrophic current from nadir altimeter or SWOT swath data, the optimal interpolation method is usually used to grid the observations with the space-time covariance function and use a percentage of the signal variance to reduce the long-wavelength error. However, this optimal interpolation method used for nadir altimeters may not be optimal for SWOT as the spatial and temporal characteristics is different. In this study, we propose to first derive the geostrophic currents in each swath from absolute dynamic topography by difference, to reduce the long-wavelength error which is constant along the tracks. And then, based on the temporal characteristics of the signal expected to be detected and high spatial SWOT observations, the spatial covariance function is used only to get the gridded geostrophic currents. The accuracy of the proposed method is verified by one year of simulated data in the Sea of Japan using MITgcm LLC4320 model and the SWOT errors. Compared with the absolute dynamic topography and geostrophic current from LLC4320 model, using the simulated data including errors, the proposed method makes high spatial sampling more effective and can obtain gridded absolute dynamic topography and geostrophic current with better accuracy especially when the number of observations is limited. In terms of the temporal variations of eddy kinetic energy, this method can significantly improve the reconstruction and detected temporal scales of mesoscale eddy variations.

1 Introduction

Satellite altimetry provided nearly 30 years of global sea level observations for ocean circulation studies since 1993. Gridding method should be used to fill the gaps between observations to satisfy the research in oceanographic applications. The optimal interpolation (OI) method of DUACS is usually used in the gridding of oceanographic observations by using their spatial and temporal correlations. However, the spatial resolution of nadir satellites is insufficient to fully observe the ocean eddies, which contain 90% of the kinetic energy of the ocean circulation (Esteban-Fernandez et al., 2010). The

https://doi.org/10.5194/egusphere-2022-1018
Preprint. Discussion started: 18 October 2022

effective spatial resolution of the DUACS-DT2018 global map, constructed with three nadir altimeters, ranges from 100 km at high latitudes to 800 km at the equator, with an average of about 200 km at mid-latitudes (Ballarotta et al., 2019). This scale is insufficient to detect the mesoscale and submesoscale features of the Kuroshio, the Mexican Warm Current and other mid-latitude western boundary currents. The mesoscale and submesoscale ocean circulation with wavelengths of 15-150 km over time is critical to understanding the role of the ocean in climate change. This part of ocean motion is one of the main channels between the inner and upper ocean, serving as both a source of energy for low-frequency geostrophic equilibrium motion, high-frequency internal tides and gravity waves, and as a destination for energy loss, and its vertical motion affects local and global heat, carbon, and nutrient cycling.

The future Surface Water and Ocean Topography (SWOT) satellite mission will be the first globally scheduled launch of a wide-swath altimetric satellite, with a repeat cycle of around 21 days, seeking to observe the ocean variability with a wavelength ranging from 15 km to 150 km. The Ka-band radar interferometric (KaRIN) and the nadir pulse-limited radar altimeter are carried to measure the sea surface simultaneously. The KaRIN measures two swaths with distance off nadir range from 10 km to 60 km on each side, and the nadir altimeter measures the along-track observations. The gap on both sides of the nadir is about 10 km, and the spatial resolution of the observation in the swath is 10-70 m, and the resolution of the sea surface height (SSH) product will be 1 km to 2 km in the open sea. Although the actual capability of SWOT for detecting ocean mesoscale and submesoscale variability is affected by measurement errors and sampling interval. The gridded SWOT SSH contains very few small mesoscale features (wavelengths < 50 km) and no submesoscale features (wavelengths < 15 km) (Gaultier et al., 2016). Compared with the nadir altimeter, the observation mode is extended from one-dimensional profile observation to two-dimensional surface observation, which can provide a large number of observations at the same time and reduce the gap between adjacent orbits. To fully exploit the capability of SWOT in improving the accuracy of the grid, the OI method used for the nadir altimeters may need to be adjusted to fit the spatial and temporal characteristics of SWOT.

In terms of the measurement errors, which affect the accuracy of the grid, in addition to the errors in the nadir altimeter, the SWOT observations are also affected by the instrument errors associated with synthetic aperture radar interferometric, including KaRIN noise, baseline dilation errors, timing errors, roll errors and phase errors. Although the geostrophic current can be calculated directly in the SWOT swath, filtering is usually required to reduce the measurement errors. For SWOT measurement errors, the effect of Laplacian diffusion filter image denoising (Gómez-Navarro et al., 2018), filtering by spatial optimal interpolation (Ma et al., 2020) and data assimilation algorithms (Metref et al., 2019) in reducing errors has been evaluated. All the above investigations reveal that the impact of noise on the along-swath geostrophic current may be controlled below 40 km wavelength after the SWOT observations are filtered, which means the filtering can control the impact of noise on the mesoscale signal. The filtering methods are usually low-pass filtering and do not involve the long-wavelength errors, which is constant along the tracks and will induce strips with sea level gradients perpendicular to the track (Le Traon et al., 1998). For SWOT observations, benefit from its two-dimensional coverage, the long-wavelength errors can be effectively removed in the difference step when calculating the geostrophic current in the swath.

https://doi.org/10.5194/egusphere-2022-1018
Preprint. Discussion started: 18 October 2022

Sampling is the other factor that affects the accuracy of the grid. The temporal sampling of T/P and Jason series satellites, which are mainly used in DUACS mapping, are a repeat period of 10 days with 254 orbits per cycle. With repeat period of ~21 days and swath width of 50 km, SWOT satellite can cover nearly the globe ocean in one cycle. However, SWOT only has a total of 292 orbits in a repeat period, which means that SWOT has fewer orbits and more observations per orbit in the same time, and will lead to an uneven temporal distribution of observations. In a 10°×10° region at mid-latitude, the number of observations from four nadir altimeters are nearly even distributed in time, while the number of observations from SWOT are unevenly distributed in time, with several days lacking observations and significant cyclical variations (Beauchamp et al., 2020). Although the combination of nadir altimeter and SWOT can ensure that observations are available every day, it does not change the uneven temporal distribution of SWOT observations. Therefore, the temporal part of the OI method used for observations of nadir altimeters, which is a Gaussian decreasing temporal function of the space-time covariance function, may not be optimal for SWOT observations.

Focus on the way of reducing long-wavelength errors and the temporal part of OI when using SWOT observations, the procedure of geostrophic currents calculating and covariance function are modified and evaluated in this study. To explore the effect of difference in reducing the long-wavelength errors, after filtering the noise, this study calculates the zonal (U) and meridional (V) geostrophic currents in the swath firstly, and then uses it as the input of OI with space-time covariance function, which is abbreviated as UV_STC. The gridded results of UV_STC are compared to the results of OI using absolute dynamic topography (ADT) as input (ADT_STC). In terms of the temporal part, since long-wavelength errors are reduced by difference, the results of OI using spatial covariance function without the Gaussian decreasing temporal function (UV_ST) are compared to that of UV_STC. Subsequently, considering that the cyclicity of the temporal distribution may impact the analysis of derived temporal variations, the possible issues of using SWOT observations to detect ocean temporal variations are analysed by taking the eddy kinetic energy variations as example.

2 Data and methods

2.1 Simulation of SWOT ADT data

The simulation of SWOT ADT consists of two parts: ADT simulation and error simulation. The ADT of LLC4320 model from Massachusetts Institute of Technology General Circulation Model is used to interpolate in the swath on both sides of nadir with a width of 50 km and a spatial resolution of 2 km. The errors are calculated by the SWOT simulator according to the specifications of the SWOT project team (Gaultier et al., 2016). The final simulated SWOT ADT data are generated by adding both of them in the Sea of Japan region for a total of 366 days from October 1, 2011 to September 30, 2012.

LLC4320 simulates the mesoscale eddy variations captured by satellite altimetry and can be used to study mesoscale eddy (Qiu et al., 2018). The temporal resolution of LLC4320 is 1 hour and the horizontal spatial resolution is 1/48°, divided into 90 layers in the vertical direction, and only the data of the top layer are used in the simulation. This model includes the full lunisolar tidal potential (Arbic et al., 2018), and the tide is a source of error in the SSH measurement, therefore, tidal

https://doi.org/10.5194/egusphere-2022-1018
Preprint. Discussion started: 18 October 2022

correction is performed using the FES2014 model. The corrected tidal components include, the four largest semidiurnal constituents (M2, S2, K2 and N2), the four largest diurnal constituents (K1, O1, P1 and Q1), and the relatively stronger components of the long period constituents (MF, MM, MSF, SA and SSA). The LLC4320 barotropic tides are 12% stronger than the reality when compared to the Harvest platform tide gauge (Zhao et al., 2019), and the semidiurnal kinetic energy associated with semidiurnal tides of model are lager by a factor of 4 compared to drifters when averaged within 60°S to 60°N (Yu et al., 2019). These overly large tidal components make the observation-based FES2014 model unable to correct the semidiurnal tides well, so the hourly data are averaged daily to attenuate the tidal influence.

The major errors impacting the SWOT signal include KaRIN noise, baseline dilation errors, timing errors, roll errors, phase errors and wet tropospheric errors. Among the instrument errors from the SWOT simulator, only KaRIN noise (Fig. 1c) is the random noise. The other instrument error is simulated based on the error power spectrum and the randomly generated phase, those error is superimposed along the track using random harmonic components and calculated to each swath according to the spatially structured of each error. In Figure 1, the timing errors (Fig. 1a) is constant across track but independent in both swaths, the baseline dilation errors (Fig. 1b) is proportional to the square of the distance to the nadir. The roll errors and phase errors are both proportional to the distance to the nadir. However, due to the roll errors and phase errors are at the decimetre level, the simulation cut off the power spectrum with wavelengths longer than 2000 km to simulate approximately the residual errors after cross-track calibrations (Fig. 1e, f). For the geophysical errors, only the residual wet tropospheric error (Fig. 1d) is generated after correction using a linear fit between the two measurements of a 2-beam radiometer.

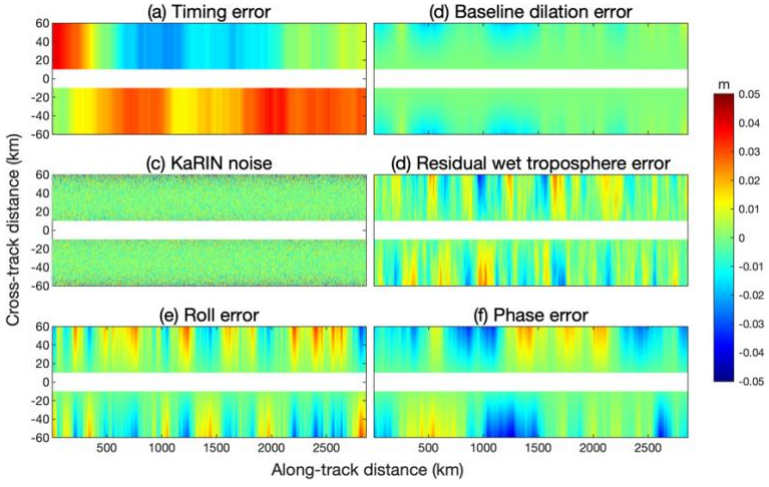

Figure 1: Instrument and geophysical errors generated by the SWOT simulator: (a) the Timing error, (b) the baseline dilation error, (c) the KaRIN noise, (d) the residual wet troposphere error, (e) the roll error and (f) phase error after cross-calibration.

https://doi.org/10.5194/egusphere-2022-1018
Preprint. Discussion started: 18 October 2022

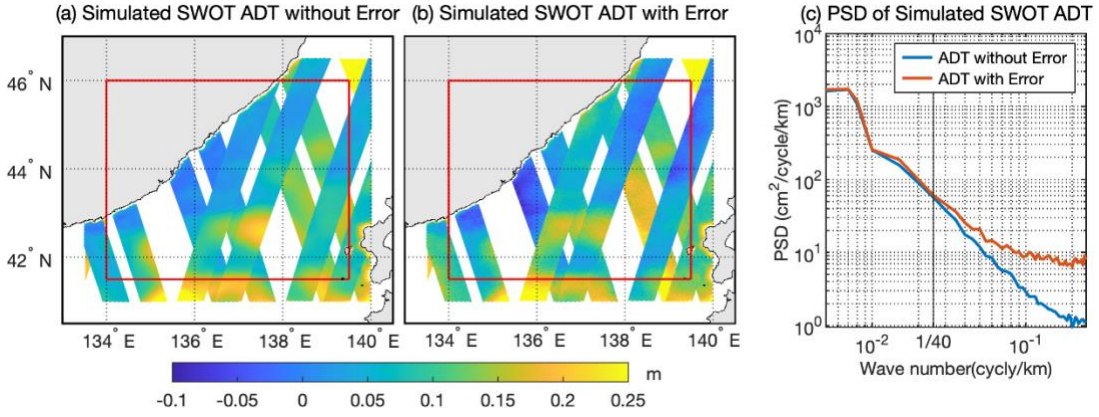

Figure 2: Simulated along-swath ADTs from Oct. 11, 2011 to Oct. 20, 2011 by LLC4320 model. (a) SWOT ADT without error. (b) SWOT ADT with errors. (c) The power spectral density (PSD) of (a) (blue line) and (b) (red line).

Figure 2 shows the distribution of the SWOT data for a subcycle during Oct. 11-20, 2011. The ADT from LLC4320 model is interpolated in the swath as shown in Fig. 2a, and is added with the simulated SWOT measurement errors as shown in Fig. 2b, which is the ADT input of OI method. Figure 2c shows the PSD of Fig. 2a and Fig. 2b, and it can be seen that, after adding the errors, although the most of spatial features of ADT can be distinguished, the wavelength less than 40 km of ADT is affected by the errors. The impact of errors and sampling will be further analysed in the region of Sea of Japan as shown in the red box (134°E~139.5°E, 41.5°N~46°N), and in order to avoid the edge effect of mapping, the area of data selection is extended outward by 0.5°.

2.2 Geostrophic current and eddy kinetic energy

The ADT is the height of the SSH relative to the geoid, and the equations for deriving the geostrophic current from ADT are expressed as follows:

$$\begin{cases} u = -\frac{g}{fR}\frac{\partial \zeta}{\partial \phi} \\ v = \frac{g}{fR\cos\emptyset}\frac{\partial \zeta}{\partial \lambda} \end{cases}, \quad (1)$$

where, $f = 2\omega \sin\phi$ is the Coriolis parameter, ω is the angular velocity of the Earth's rotation, ω is the meridional direction, λ is the zonal direction, ζ is the ADT, u and v is the zonal and meridional geostrophic current, respectively, g is the acceleration of gravity. In practice, the derivatives of ADT are usually calculated by differencing the ADT over discrete grid points.

The eddy kinetic energy (EKE) is widely used as the index for evaluating eddy variations. It is calculated by

$$EKE = \frac{u'^2 + v'^2}{2}, \quad (2)$$

where u' and v' is the velocity anomalies from the mean velocity of u and v, respectively.

https://doi.org/10.5194/egusphere-2022-1018
Preprint. Discussion started: 18 October 2022

Geostrophic balance explains over 80% of variance in high kinetic energy regions such as the Western Boundary Current and the Antarctic Circumpolar Current (Yu et al., 2021), and dominates at time scales greater than 3 to 10 days and at spatial scales longer than 50 km (Lee and Kim, 2021). Therefore, the unbalanced wave motion of mesoscale eddy variations is not considered in this study, the EKE is calculated from geostrophic current. Considering the importance of the seasonal variation of mesoscale eddies and the repeat period of SWOT satellite is about 3 weeks, this study decomposes the time series of EKE into the linear variation, seasonal variation with 13 weeks, 3-13 weeks variation, and residual variation with cycle smaller than 3 weeks, and analyses the reconstruction results on the characteristics of EKE variations with different cycles.

2.3 The optimal interpolation method

The OI method can be used for the mapping of discrete ADT data from satellite altimetry, which is essentially a minimum variance estimation. When there is a linear relationship between the input and the output of the minimum variance estimation, the unbiased estimation of the output can be obtained based on the principle of linear minimum variance estimation, using the priori mathematical expectation, variance and covariance. Its estimation criterion is the minimum mean squared error of the output, and the output is given by

$$X = \mu_X + D_{XY} {D_{YY}}^{-1} (Y - \mu_Y) \,, \tag{3}$$

where, X is the output, Y is the input, μ_X and μ_Y are their mathematical expectations, respectively, D_{XY} is the cross-covariances matrix of output and input, D_{YY} is the covariance matrix of input. In this study, Y is the discrete observation of ADT or zonal (U) and meridional (V) geostrophic current in the swath, X is the gridded ADT. Since the mathematical expectation of the input and output is difficult to obtain precisely, the mean value of the input, the iterative grid value, or the steady-state model can be used to make the mathematical expectation zero in OI.

When the input is ADT, the first relationship between Y and X is bilinear interpolation, while when the input is zonal (U) and meridional (V) geostrophic current, the second relationship between Y and X is based on the former, combined with Eq. (1), which can be linearized by the difference method, therefore, the second relationship is also linear. As a result, we can assume the following equation between Y and X:

$$Y = HX + \varepsilon \,, \tag{4}$$

where H is the linear relationship between Y and X, ε is the error of discrete observations. By adopting Eq. (4), Eq. (3) becomes a tractable form with mathematical expectation is zero (Qiu et al., 2016)

$$X = ({D_{XX}}^{-1} + H^T {D_{\varepsilon\varepsilon}}^{-1} H)^{-1} H^T {D_{\varepsilon\varepsilon}}^{-1} Y \,, \tag{5}$$

where, D_{XX} is the covariance matrix of X, $D_{\varepsilon\varepsilon}$ is the covariance matrix of ε. The correlation of errors among discrete observations is not considered in this study, so $D_{\varepsilon\varepsilon}$ is a diagonal matrix.

https://doi.org/10.5194/egusphere-2022-1018
Preprint. Discussion started: 18 October 2022

D_{XX} is given by the autocovariance function:

$$C(r,t) = \sigma_X^2 \left[1 + \frac{r}{L_{xy}} + \frac{1}{6}\left(\frac{r}{L_{xy}}\right)^2 - \frac{1}{6}\left(\frac{r}{L_{xy}}\right)^3\right] \exp\left(-\frac{r}{L_{xy}}\right) \exp\left(-\frac{t^2}{L_t^2}\right), \quad (6)$$

where, r and t is the spatial and temporal distance between any two points of X, respectively, σ_X^2 is the variance of X, L_{xy} and L_t is the decorrelation scale in space and time, respectively, according to the partial autocorrelation results of the LLC4320 model in the study area, $L_{xy} = 27\ km$ and $L_t = 3.6\ days$. This space-time covariance function is based on the spatial covariance function of Arhan & Verdiére (1985), added with the additional Gaussian decreasing temporal function $\exp(-t^2/{L_t}^2)$. While the long-wavelength signal of sea level change can be reduced as long-wavelength errors, and the short-wavelength signal with temporal scales of a few days is mainly submesoscale eddy, which is undetectable and neglectable to mesoscale eddy. Therefore, the observations within a time window of ±5 days is assumed as the observations of the central day in the UV_SC method, and only the spatial covariance function is needed.

2.4 The filtering and accuracy evaluation method

The geostrophic current derived from the simulated SWOT ADT without error is shown in Fig. 3a, the geostrophic current has obvious gross errors due to the data missing in coastal areas. To reduce the impact of gross errors, the data within 20 km from the coastline are excluded in subsequent processing using A Global Self-consistent, Hierarchical, High-resolution Geography (GSSHG) database. In Fig. 3b, the geostrophic current is calculated from the simulated SWOT ADT with error, it can be seen that the impact of the SWOT error to the geostrophic current is amplified after the derivation, and the characteristics of geostrophic current are difficult to detect due to the effect of noise. In addition, the PSD (Fig. 3d) shows that the wavelength of the geostrophic current affected by the noise is reduced from 40 km for ADT to 100 km, and makes the geostrophic current with wavelength less than 100 km similar to Gaussian white noise, and the PSD tends to be constant. Therefore, before calculating geostrophic current, filtering is required to reduce the high frequency noise.

https://doi.org/10.5194/egusphere-2022-1018
Preprint. Discussion started: 18 October 2022

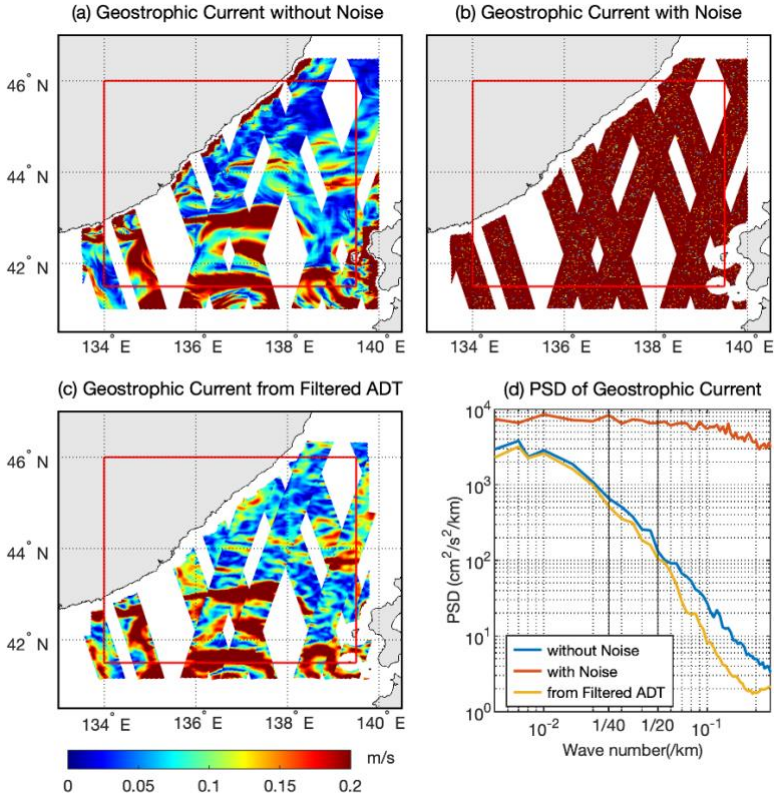

Figure 3: The Geostrophic current from Oct. 11, 2011 to Oct. 20, 2011 and their PSDs from simulated SWOT ADTs. (a) Geostrophic current without noise. (b) Geostrophic current with noise. (c) Geostrophic current derived from filtered ADT using Gaussian filtering. (d) PSDs of (a) (blue line), (b) (red line) and (c) (yellow line).

The low-pass Gaussian filter is used here for noise processing. Gaussian filter is a linear smoothing filter, which reduces the noise at the calculation point by weighting the data within a filtering radius of the calculation point as follows:

$$h_g = \frac{\sum_{i=1}^{m} w_i h_i}{\sum_{i=1}^{m} w_i}, \tag{7}$$

where, h_g is the filtered ADT at the calculation point, m is the total number of selection points within the radius, h_i is the ADT of the selection point within the radius, w_i is the weight of the selection points given by

$$w_i = \frac{1}{\sqrt{2\pi}\sigma} \exp\left(-\frac{d_i^2}{2\sigma^2}\right), \tag{8}$$

where, d_i is the geodesic distance from the selection point to the calculation point, σ is the standard deviation of the Gaussian distribution, which is taken as 1/3 of the filtering radius.

To analyse the accuracy of the filtered geostrophic current and reconstructed EKE variations (S_{af}) computed from simulated data, using the geostrophic current and EKE variations (S_{true}) computed from the model as reference, following the principle of relative error, the error-signal ratio of RMS, denoted by RRMSE, is used to express the impact of the error on the signal. It is defined as follows:

https://doi.org/10.5194/egusphere-2022-1018
Preprint. Discussion started: 18 October 2022

$$RRMSE = \frac{rms(S_{af} - S_{true})}{rms(S_{true})}, \quad (9)$$

3 Results and discussion

3.1 Effect of difference in reducing long-wavelength errors

A Gaussian filter with a radius of 14 km is applied to each swath in Fig. 2b to obtain filtered ADT, Fig. 3c shows the geostrophic current derived from the filtered ADT, and its PSD is the yellow line as shown in Fig. 3d. The filtering reduced the noise of the geostrophic current at wavelengths longer than 40 km and also have effect on the noise in the 20 km to 40 km wavelength range as shown in Fig. 3. To evaluate the accuracy, the simulated SWOT ADT with error from October 1, 2011 to September 30, 2012 is filtered with a 14 km radius and geostrophic current is derived, and then it is compared with the noiseless geostrophic current calculated from the simulated SWOT ADT without error during the same period. The statistical results are shown in Table 1, the RMSE of the geostrophic current from filtered ADT is about 0.05m/s, which is very close to the RMSE (0.0328m) of the simulated SWOT ADT with errors. The RRMSE is about 0.4, and the spatial correlation with the noiseless geostrophic current is larger than 0.8. Therefore, it is assumed that filtering can effectively reduce the noise and recover the mesoscale signal of geostrophic current, it is reliable to using the zonal (U) and meridional (V) geostrophic currents as input.

Table 1: The statistical results of the geostrophic current derived from the filtered ADT in the swath, from October 1, 2011 to September 30, 2012

	RMSE(m/s)	RRMSE	Correlation Coefficient
Geostrophic Current	0.0548	0.33	0.87
U	0.0558	0.41	0.91
V	0.0519	0.54	0.84

A time window of ±5 days is selected to obtain the daily ADTs on a 0.1° grid on May 27, 2012 using the ADT_STC (Fig. 4b) and UV_STC (Fig. 4c) method, respectively. The error (Fig. 4d, e) of them is calculated by ADT (Fig. 4a) from LLC4320 model on the same day, respectively. In Fig. 4d, the track of SWOT with an orbit inclination of 77.6° and a width of 120 km is visible, and the strip caused by the long-wavelength error along track expands to both sides. The scale of this strip reaches almost 200 km in the zonal direction and 800 km (estimated by the orbit inclination) in the meridional direction, which is the scale of mesoscale signal. Benefiting from the fact that the long-wavelength error is constant along track, and the difference process of deriving the zonal (U) and meridional (V) geostrophic currents can remove the constant terms, therefore, the long-wavelength errors could be removed effectively in the UV_STC method as shown in Fig. 4e.

https://doi.org/10.5194/egusphere-2022-1018
Preprint. Discussion started: 18 October 2022

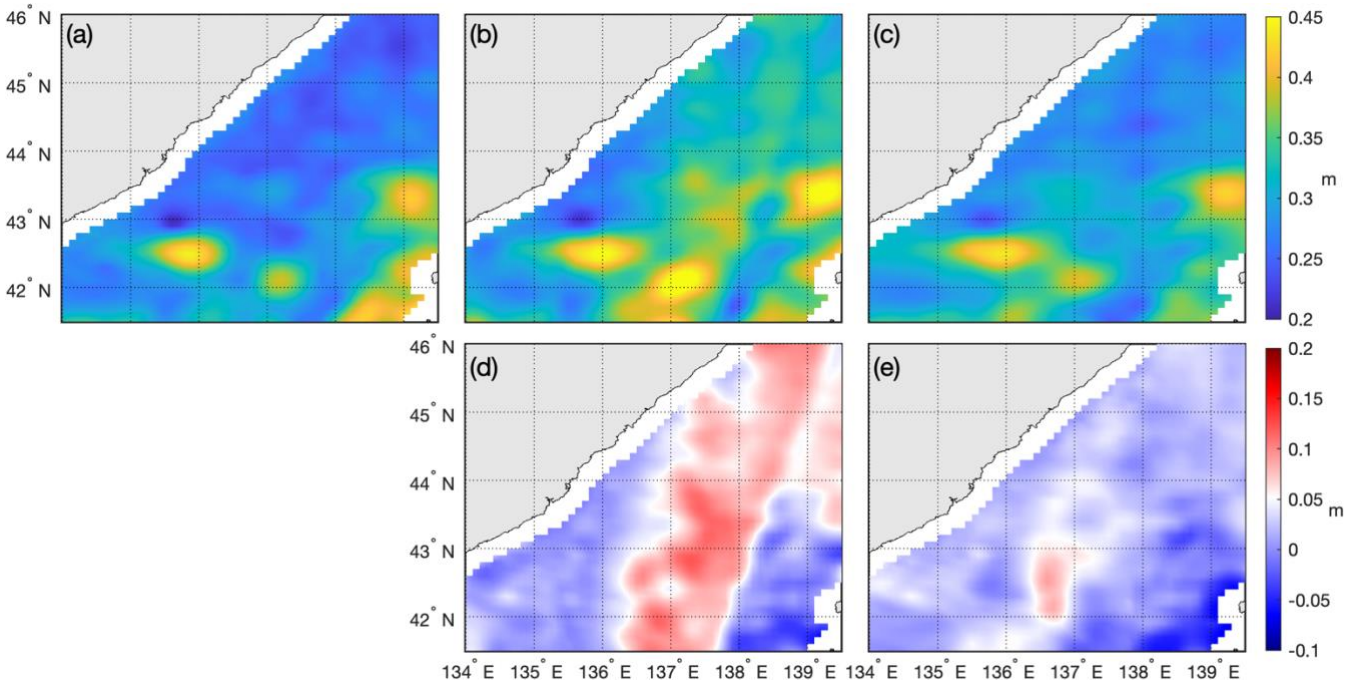

Figure 4: Comparison of ADT using ADT_STC and UV_STC method on May 27, 2012. (a) The ADT of model; (b) The ADT calculated by ADT_STC method and its error (d) related to (a); (c) The ADT calculated by UV_STC method and its error (e) related to (a).

3.2 Accuracy of gridded ADT and geostrophic current

The daily ADTs of the UV_SC and UV_STC method is gridded with a time window of ±5 days on a 0.1° grid, respectively, and then averaged weekly during these 49 weeks from October 11, 2011 to September 17, 2012. The ADT from LLC4320 model is resampled and averaged into the same spatial and temporal resolution during the same period, which are used as references. The gridded geostrophic current is also derived from those gridded ADTs.

https://doi.org/10.5194/egusphere-2022-1018
Preprint. Discussion started: 18 October 2022

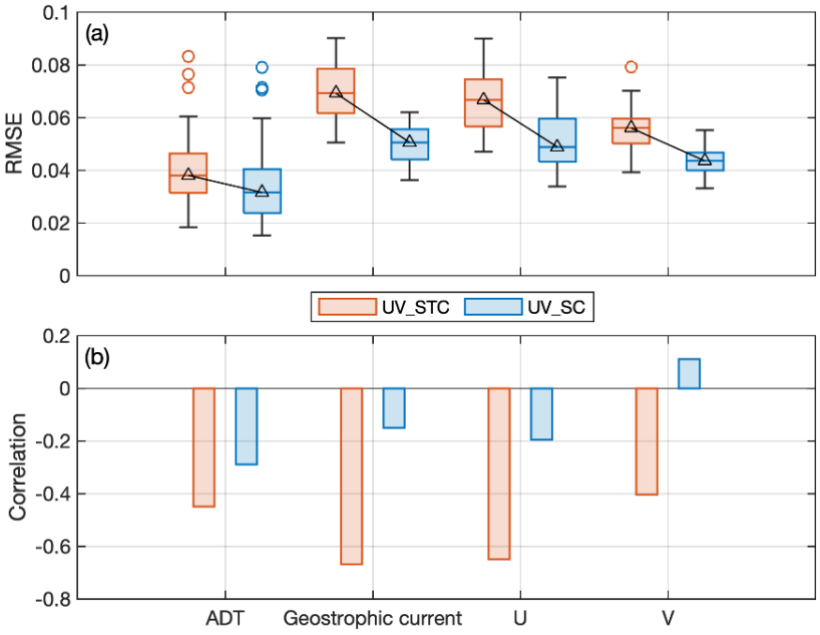

Figure 5: Statistics of weekly gridded results using UV_STC and UV_SC method. (a) Box chart of weekly RMSE for gridded results using UV_STC and UV_SC methods during the 49 weeks, respectively. (b) Bars of Correlation coefficients between the weekly RMSE of each result in (a) and the number of observations per week.

The RMSE of weekly gridded results using UV_STC and UV_SC method are calculated, respectively, and the box chart of the weekly statistical results during the 49 weeks are shown in Fig. 5a. The RMSE of UV_SC are lower than that of UV_STC, especially for geostrophic current, and have relatively concentrated distribution for geostrophic current, which may indicate that UV_SC is more robust than UV_STC on the overall. In Fig. 5b, it is obvious that the correlation coefficients between the RMSE of UV_STC and the number of observations per week is significant, which is amplified from ADT to geostrophic current. However, the correlation coefficients of UV_SC is lower than 0.3. Therefore, it can be assumed that the improvement of UV_SC over UV_STC comes from the fact that UV_SC is less influenced by the number of observations per week.

Comparing the gridded zonal (U) and meridional (V) geostrophic current of the same method, the RMSE of meridional (V) geostrophic current is better than that of zonal (U) geostrophic current in both methods as the slight difference of them about RMSE in Table 1. Considering that the orbital inclination of the SWOT satellite is greater than 45° and the simulated error has smaller change across the orbit than along the orbit as shown in Fig 1, it can be assumed that the zonal component of the SWOT error varies smaller than the meridional component. The meridional (V) geostrophic current is derived from the zonal ADT caused by the Coriolis force, therefore, although SWOT has more features in the meridional direction, the zonal (U) geostrophic current has higher noise than the meridional (V) geostrophic current. It may indicate that using the meridional (V) geostrophic current only as input may improve the accuracy of gridded ADT.

https://doi.org/10.5194/egusphere-2022-1018
Preprint. Discussion started: 18 October 2022

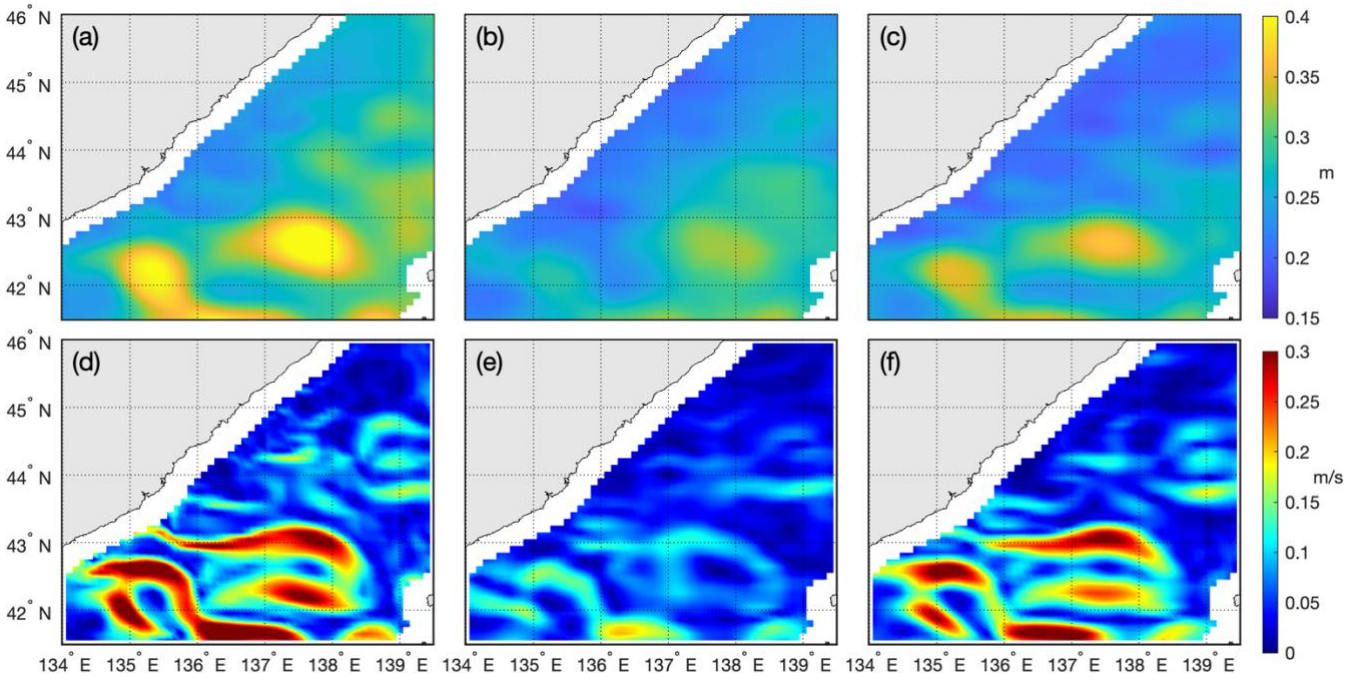

Figure 6: The gridded ADTs and geostrophic currents in the 1st week, Oct. 11-17, 2011. (a), (b) and (c) are ADTs of model, UV_STC and UV_SC, respectively; (d), (e) and (f) are geostrophic currents derived from (a), (b) and (c), respectively.

For further analysis, the grid results of the 1st week are used, where the RMSE of gridded geostrophic current has largest improvement from UV_STC to UV_SC during the 49 weeks, and the number of observations in this week is also the least. The gridded ADT and geostrophic current calculated by UV_STC and UV_SC underestimate the gridded results of model as shown in Fig. 6. The Gaussian decreasing temporal function in the UV_STC method will make the gridded results closer to the observations within the decorrelation scale in time, which may insufficient to describe the reality due to the insufficient temporal sampling, leading to the gridded results of UV_ STC have more obvious underestimation and less accuracy. The UV_SC method can better reduce the effect of insufficient temporal sampling compared to the UV_STC method. This indicates that the lack of observations has greater impact then the difference between the observations in a window of ±5 days, at least in this region.

3.3 Temporal variations of reconstructed mesoscale eddy

The EKE of UV_SC and UV_STC are calculated and compared with the EKE of model to evaluate the accuracy of the two methods in investigating the temporal variations of mesoscale eddy. The first step is to average the EKE spatially in the study area to calculate the EKE time series as shown in Fig. 7a, then perform a linear fit to obtain and remove the linear

https://doi.org/10.5194/egusphere-2022-1018
Preprint. Discussion started: 18 October 2022

variation, and performing a 13 weeks low-pass filter to obtain the EKE seasonal variation (Fig. 7b), after removing the previous variations and applying a 3 week low-pass filter, the EKE 3-13 week variation (Fig. 7c) and the EKE residual variation with cycle less than 3 weeks (Fig. 7d) are separated.

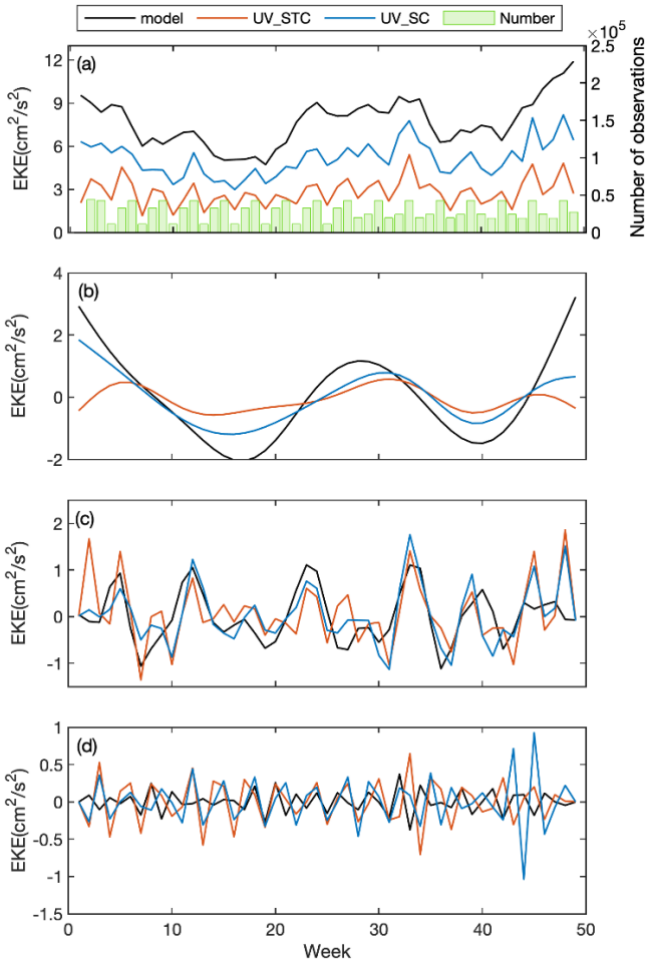

290 **Figure 7: Temporal variations of EKE. (a) Time series, (c) seasonal variation, (e) 3-13 weeks variation, and (g) residual variation of EKE are calculated by model (black lines), UV_STC (orange lines) and UV_SC (blue lines) in the study area. The number of observations per week are provided by the green bars in (a)**

In Fig. 7a, the time series of UV_STC has a significant deviation compared to that of model, and this deviation is reduced by
295 UV_SC as shown in Fig. 6. In Fig. 8, the correlation between the time series of UV_SC and UV_STC and the time series of model are 0.823 and 0.487, respectively, and the time series of UV_STC also has a higher RRMSE than the time series of UV_SC, which indicates that UV_SC can better reconstruct the temporal variations of mesoscale eddy. Specifically, the number of observations per week in the study area has a 3-week variation (see the green bars in Fig. 7a) as the repeat period of SWOT, and the correlation between the 3-week variation and the time series of model, UV_SC and UV_STC are -0.039,

https://doi.org/10.5194/egusphere-2022-1018
Preprint. Discussion started: 18 October 2022

0.261 and 0.649, respectively. This indicates that the time series of both UV_SC and UV_STC has an extra variation associated with the 3-week variation compared to the time series of model, especially for UV_STC. Therefore, the seasonal variations of both methods have a higher correlation due to the 3-week variation is filtered. However, although the UV_STC method can reconstruct the seasonal variation with a correlation of 0.549, the 3-week variation still interferes with the extraction of seasonal variation from 1st week to 5th week, and the RRMSE almost reaches 1, while the UV_SC method reconstruct the seasonal variation better.

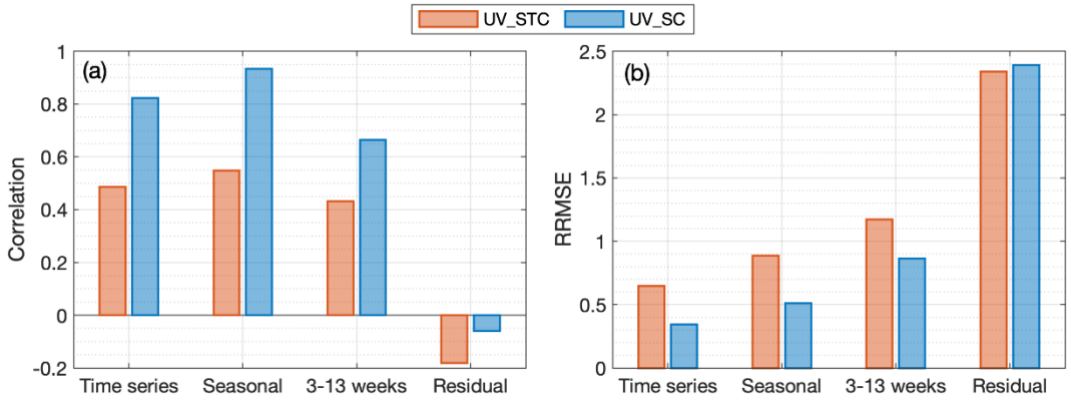

Figure 8: Statistics of variations calculated by UV_STC and UV_SC method. (a) The correlation coefficients between each variation of both methods and model, and (b) RRMSE of each variation.

On the 3-13 weeks variation, the 3-week variation dominates this variation of UV_STC, resulting in an RRMSE greater than 1 even though the correlation is 0.431. The UV_SC method is less affected by the 3-week variation and still has an RRMSE less than 1 and a correlation larger than 0.6. On the residual variation with cycle less than 3 weeks, the correlation and RRMSE of both methods show that neither of both methods can reconstruct this variation. In addition, the RRMSE of UV_STC and UV_SC are both growing as the cycle of variations decreases as shown in Fig. 8b, therefore, the variations are not reconstructed well with small cycles. In general, comparison of the correlation and RRMSE of the two methods indicates that UV_SC has an increased capability to reconstruct each variation than UV_STC.

4 Conclusion

The application of SWOT data is challenging with its limited temporal sampling and new type of measurement errors. In this study, one year of SWOT ADT observations are simulated in the Sea of Japan region using MITgcm LLC4320 ADT data and the errors from SWOT simulator. To adapt with the spatial and temporal characteristics of SWOT swath observations. According to the spatial characteristics of SWOT, we propose to use the zonal (U) and meridional (V) geostrophic current obtained after filtering in the swath as input of OI, the inconsistency of observations between satellite ground tracks is then

https://doi.org/10.5194/egusphere-2022-1018
Preprint. Discussion started: 18 October 2022

eliminated, the long-wavelength error could be reduced effectively with the difference process. In addition, based on the spatial characteristics of measurement errors, using meridional (V) geostrophic current only as input may improve the accuracy.

With the insufficient temporal sampling and the small decorrelation scale in time, the Gaussian decreasing temporal function of OI method needs to be improved, to reduce the effect of insufficient temporal sampling. Within the time window of ±5 days, the sea level change could be neglected, therefore, the improvement of removing the Gaussian decreasing temporal function in the UV_SC method works. Furthermore, as the large number of observations from SWOT can improve the accuracy of grid results, the accuracy is highly related to the uneven temporal distribution. Using the EKE variations as example, a 3-week variation caused by the number of observations per week affects the reconstruction of the EKE variations, resulting in only the UV_SC method can reconstruct the variations from 3 to 13 weeks. Furthermore, benefit from less effect of 3-week variations, the seasonal variations can be better reconstructed by UV_SC method than UV_STC method.

Considering the correlation between the number of observations and the accuracy of gridded results, for detecting the temporal variations, the temporal resolution of gridded results probably should be 10 days, which is the subcycle of SWOT and observations are evenly distributed on this scale. Just as C3S chose to use only two nadir altimeters when mapping to ensure the stability of mean sea level, it may be worthwhile to sacrifice a certain spatial resolution in the design of the satellite to reduce the uneven temporal distribution of observations, in order to ensure the stability of reconstructed temporal variations.

Code and data availability

The SWOT simulator can be found at https://github.com/CNES/swot_simulator. LLC4320 data is available at https://data.nas.nasa.gov/ecco/data.php. FES2014 was produced by Noveltis, Legos and CLS and distributed by Aviso+, with support from CNES https://www.aviso.altimetry.fr/. GSSHG database is available at http://www.soest.hawaii.edu/wessel/gshhg/.

Author contributions

TJ and XW initiated the study. JS and MZ performed the data simulation. JS proposed and completed the method. TJ, WJ and XW discussed and suggested the results. JS and TJ wrote the manuscript with the help of other authors.

Competing interests

The authors declare that they have no conflict of interest.

https://doi.org/10.5194/egusphere-2022-1018
Preprint. Discussion started: 18 October 2022

Acknowledgements

This study is supported by National Natural Science Foundation of China under Grants 41974020, 42192531 and 41721003, the Special Fund of Hubei Luojia Laboratory and Foundation of Shanghai Academy of Spaceflight Technology under grant SAST2020-035.

References

Arbic, B. K., Alford, M. H., Ansong, J. K., Buijsman, M. C., Ciotti, R. B., Farrar, J. T., Hallberg, R. W., Henze, C. E., Hill, C. N., Luecke, C. A., Menemenlis, D., Metzger, E. J., Müeller, M., Nelson, A. D., Nelson, B. C., Ngodock, H. E., Ponte, R. M., Richman, J. G., Savage, A. C., Scott, R. B., Shriver, J. F., Simmons, H. L., Souopgui, I., Timko, P. G., Wallcraft, A. J., Zamudio, L., and Zhao, Z.: A Primer on Global Internal Tide and Internal Gravity Wave Continuum Modeling in HYCOM and MITgcm, in: New Frontiers in Operational Oceanography, edited by: Chassignet, E. P., Pascual, A., Tintoré, J., and Verron, J., GODAE OceanView, 307–392, https://doi.org/10.17125/gov2018.ch13, 2018.

Arhan, M. and Verdiére, A. C. D.: Dynamics of Eddy Motions in the Eastern North Atlantic, Journal of Physical Oceanography, 15, 153–170, https://doi.org/10.1175/1520-0485(1985)015<0153:DOEMIT>2.0.CO;2, 1985.

Ballarotta, M., Ubelmann, C., Pujol, M.-I., Taburet, G., Fournier, F., Legeais, J.-F., Faugère, Y., Delepoulle, A., Chelton, D., Dibarboure, G., and Picot, N.: On the resolutions of ocean altimetry maps, Ocean Science, 15, 1091–1109, https://doi.org/10.5194/os-15-1091-2019, 2019.

Beauchamp, M., Fablet, R., Ubelmann, C., Ballarotta, M., and Chapron, B.: Intercomparison of Data-Driven and Learning-Based Interpolations of Along-Track Nadir and Wide-Swath SWOT Altimetry Observations, Remote Sensing, 12, 3806, https://doi.org/10.3390/rs12223806, 2020.

Esteban-Fernandez, D., Fu, L.-L., Rodriguez, E., Brown, S., and Hodges, R.: Ka-band SAR interferometry studies for the SWOT mission, in: 2010 IEEE International Geoscience and Remote Sensing Symposium, 2010 IEEE International Geoscience and Remote Sensing Symposium, 4401–4402, https://doi.org/10.1109/IGARSS.2010.5652302, 2010.

Gaultier, L., Ubelmann, C., and Fu, L.-L.: The Challenge of Using Future SWOT Data for Oceanic Field Reconstruction, Journal of Atmospheric and Oceanic Technology, 33, 119–126, https://doi.org/10.1175/JTECH-D-15-0160.1, 2016.

Gómez-Navarro, L., Fablet, R., Mason, E., Pascual, A., Mourre, B., Cosme, E., and Le Sommer, J.: SWOT Spatial Scales in the Western Mediterranean Sea Derived from Pseudo-Observations and an Ad Hoc Filtering, Remote Sensing, 10, 599, https://doi.org/10.3390/rs10040599, 2018.

Le Traon, P. Y., Nadal, F., and Ducet, N.: An Improved Mapping Method of Multisatellite Altimeter Data, J. Atmos. Oceanic Technol., 15, 522–534, https://doi.org/10.1175/1520-0426(1998)015<0522:AIMMOM>2.0.CO;2, 1998.

Lee, E. A. and Kim, S. Y.: A diagnosis of surface currents and sea surface heights in a coastal region, Continental Shelf Research, 226, 104486, https://doi.org/10.1016/j.csr.2021.104486, 2021.

Ma, C., Guo, X., Zhang, H., Di, J., and Chen, G.: An Investigation of the Influences of SWOT Sampling and Errors on Ocean Eddy Observation, Remote Sensing, 12, 2682, https://doi.org/10.3390/rs12172682, 2020.

https://doi.org/10.5194/egusphere-2022-1018
Preprint. Discussion started: 18 October 2022

Metref, S., Cosme, E., Le Sommer, J., Poel, N., Brankart, J.-M., Verron, J., and Gómez Navarro, L.: Reduction of Spatially Structured Errors in Wide-Swath Altimetric Satellite Data Using Data Assimilation, Remote Sensing, 11, 1336, https://doi.org/10.3390/rs11111336, 2019.

Qiu, B., Chen, S., Klein, P., Ubelmann, C., Fu, L.-L., and Sasaki, H.: Reconstructability of Three-Dimensional Upper-Ocean Circulation from SWOT Sea Surface Height Measurements, Journal of Physical Oceanography, 46, 947–963, https://doi.org/10.1175/JPO-D-15-0188.1, 2016.

Qiu, B., Chen, S., Klein, P., Wang, J., Torres, H., Fu, L.-L., and Menemenlis, D.: Seasonality in Transition Scale from Balanced to Unbalanced Motions in the World Ocean, Journal of Physical Oceanography, 48, 591–605, https://doi.org/10.1175/JPO-D-17-0169.1, 2018.

Yu, X., Ponte, A. L., Elipot, S., Menemenlis, D., Zaron, E. D., and Abernathey, R.: Surface Kinetic Energy Distributions in the Global Oceans From a High-Resolution Numerical Model and Surface Drifter Observations, Geophysical Research Letters, 46, 9757–9766, https://doi.org/10.1029/2019GL083074, 2019.

Yu, X., Ponte, A. L., Lahaye, N., Caspar-Cohen, Z., and Menemenlis, D.: Geostrophy Assessment and Momentum Balance of the Global Oceans in a Tide- and Eddy-Resolving Model, Journal of Geophysical Research: Oceans, 126, e2021JC017422, https://doi.org/10.1029/2021JC017422, 2021.

Zhao, Z., Wang, J., Menemenlis, D., Fu, L.-L., Chen, S., and Qiu, B.: Decomposition of the Multimodal Multidirectional M2 Internal Tide Field, Journal of Atmospheric and Oceanic Technology, 36, 1157–1173, https://doi.org/10.1175/JTECH-D-19-0022.1, 2019.